

BUCKLING ANALYSIS OF PRE-LOADED IMPERFECTION SENSITIVE SPHERICAL SHELL SUBJECTED TO IMPACT LOADS

Thani Aswanth, me19mtech11025

March 2020

1 Introduction

1.1 Overview

A shell is a body surrounded by two parallel curving surfaces that are closely spaced. The Shape of shell structure can be defined even At every area, we just know the calculation of the focal surface and the shell thickness. The region between two concentric spheres of differing radii is a spherical shell. A thin shell is a shell where radius to thickness ratio is small compared to unity. Every part of a structure or machine is a three-dimensional body irrespective of how small the dimension maybe. If the shell has maximum rise to base diameter ratio of a shell is very small, then the shell is considered to be shallow.



Figure 1: Spherical shells used as storage tanks

Shell structures are utilized in a different fields, including aviation, atomic, marine, and petrochemical. Shells are commonly used in sophisticated components such as missiles, space vehicles, submarines, nuclear reactor vessels, and refinery equipment. The spherical shells are mostly used as a spherical cap or a hemisphere. Particularly spherical shell structures have a wide scope of primary applications in designing. Spherical shells can be used as storage tanks. The spherical submarine is a typical example of spherical shells under hydrostatic pressure. Shell caps a portion of a complete spherical shell, are most commonly caps used as concrete roofs. Precisely gauge the maximum buckling load in all cases to avoid catastrophic failure and improve the scope of working conditions.

Compressive membrane forces may cause the shells to collapse owing to buckling or compressive instability whenever they are subjected to varied loading situations such as external pressure and heat loads. Under



Figure 2: Manned submarine in spherical shell shape used to probe ocean depths

axial load, cylindrical shells and spherical shells under external pressure, buckling occurrences cause a rapid reduction in load bearing capability, displays severe nonlinear behaviour after buckling happens and the load carrying capacity decreases. Both of these shell loading combinations are very failure prone, with loads which causes buckling phenomena are as less as 20% of the ideal shell's load bearing capability experimentally observed.



Figure 3: Kresge Auditorium of MIT with roof of shell structure

1.2 Literature Review

Euler worked on solving the instability problems based upon lateral buckling of compressed members about 200 years ago by. During that time the common structural materials were wood and stone. Because of the low strength of these materials, elastic stability isn't a major concern. Theoretical solution developed by Euler for slender bars was not in application for a long time. Only after the widespread use of steel in the construction of railway bridges does the issue of compression member buckling become realistic.

Von Karman and Tsien (1939) [1] showed that usually shell-like structures are susceptible to compression loading. As a result, even a minor disturbance could force them to snap into a distorted position. In their article, they sought to explain why experimental and theoretical buckling pressures for fixed spherical shells which are not that much deep, under uniform pressure differed.

Koiter (1945) [2] made significant contribution by establishing hypothesis on elastic system under load which is conservative. He used a procedure to link the early states after buckling taking place with the susceptibility to defects in this paper. However, the imperfection sensitivity forecasts are only valid for minor imperfections.

Hutchinson (1967) [3] the behaviour immediately after buckling of a not that deep sections of a spherical shell exposed to external load was examined. According to his results, imperfections in shell geometry have a similar adverse influence on buckling strengths of spherical shells as they do on axially compressed cylindrical shells.

Hutchinson (2016) [4] introduced middle surface imperfections such as dimple shaped imperfections in the spherical shell surface and made new findings like buckling mode localization which occurs immediately

after buckling and lower limit for buckling for large imperfections.

1.3 Spherical shell Buckling

Shell buckling problem has always been difficult to solve in mechanics field. Zoelly (1915) [5] for the first time, the maximum buckling load of a thin spherical shell under continuous external pressure over the surface was calculated. The critical buckling load is determined using linear buckling analysis, which involves finding the minimum eigen values of a set of equations.

$$p_c = \frac{2E}{\sqrt{3(1-\nu^2)}} \left(\frac{t}{R} \right)^2 \quad (1)$$

Where E is the Young's modulus, ν is the Poisson's ratio and shell radius is R and thickness of shell is t. The above equation for perfect shell is very inaccurate approximation of experimental buckling load and large discrepancies were found in experimental and critical buckling load values. In the latter half of the twentieth century, a great number of tests on spherical shells were carried out in order to better understand the buckling behaviour of shells under uniform pressure. The buckling outcomes are often expressed by so-called knockdown factors, This is the ratio of the shell's highest buckling load to its critical buckling load as determined by classical buckling theory.

$$\kappa_d = \frac{p_{max}}{p_c} \quad (2)$$

Whenever a uniform external pressure is applied on spherical shell it buckles at much lower pressure than critical buckling pressure. From the data of various experimental studies, it was found out that knockdown value reduces as the radius-to-thickness ratio rises. spherical shells which are made with very less precision collapse at lower critical pressure values ($0.17 < \kappa_d < 0.8$) than theoretically predicted. Shells manufactured with great accuracy by machining aluminium tend to have higher maximum pressures ($0.45 < \kappa_d < 0.9$).The majority of these tests were carried out on shallow spherical shells. Explanation for discrepancy between experimental and theoretical values was proposed by (von Kármán, 1939][1]; von Kármán et al., 1940 [6]; von Kármán and Tsien, 1941 [7]).

The comprehensive theory of elastic stability proposed by Koiter, which linked defect susceptibility to the behaviour at initial phase after buckling happens for entire spheres under external pressure, was shown to be true only for extremely minute imperfections too low to be represented on real shells.

1.4 Imperfection sensitivity of shell buckling

Fig.4 represents load-displacement behaviour of shell such as spherical shell under uniform pressure [8]. Loading may proceed in a straight line. Along this route, the OA distorted shape remains the same, but the magnitude of displacement grows. Along the OA path, there are axisymmetric deformations. Maximum load is reached at A and is termed as limit point load or critical buckling load path OA is primary equilibrium path. For spherical shell under uniform compression an equilibrium path is available a bifurcation point exists at B where two equilibrium paths are possible first an axisymmetric deformed shape path OA and second an asymmetric deformed shape along BD it is called bifurcation buckling or post buckling path. Initially in post buckling path lobes are formed around the circumference of shell.

Almost all the shell structures are imperfect. Shell structures contain deviations in geometry and material of construction can also be non-homogenous, Residual stresses during fabrication methods such as welding etc for such structures load-displacement path follows OEF and buckling load corresponds to point E deformation mode at E will include both symmetric and asymmetric components

1.5 Simulation of Buckling in ABAQUS

Buckling is highly nonlinear phenomenon; large deformations take place, making it difficult to study using analytical methods. Numerical methods are very helpful to study buckling and Finite element analysis (FEA) is one of the popular method. ABAQUS FEA package has been used in this project. Buckling is mainly instability problem which can be simulated in ABAQUS using static procedure Riks method. The Riks technique is used to forecast the unpredictability of a geometrically nonlinear structure's collapse. Riks

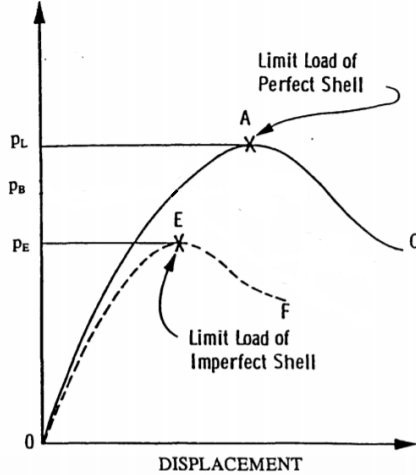


Figure 4: Load deflection curve indicating post buckling paths

technique treats both load and displacement as unknowns, and employs another parameter, "arc length," to track the development of the solution. This procedure produces a solution even if the solution is stable or unstable.

1.6 Linear perturbation Buckling

Eigenvalue is a term that is used to estimate the maximum buckling load of rigid structures. Before buckling happens structures with high stiffness normally experience very small amount of deformation. The Euler column is an example of stiff structure because its response to compressive load is very stiff until a critical load is achieved, at which point it bends abruptly and exhibits substantially decreased stiffness. In eigenvalue buckling analysis we estimate loads at which model stiffness matrix becomes singular.

$$k^{MN}v^M = 0 \quad (3)$$

k^{MN} is the tangent stiffness matrix and v^M are nontrivial displacements when loads are applied. Eigen value buckling analysis provides crucial estimates of collapse mode shapes.

1.7 Static Riks method

When the load-displacement response has a negative stiffness, the structure must release strain energy to maintain equilibrium resulting in collapse behaviour. Even when the load decreases as the displacement increases, displacement adjustment can give a solution in certain situations. An automated version of this static analysis process is available in Abaqus/Standard. This method is called static Riks method [9]. There is a continuation of a prior history in Riks method. The load at the beginning of the step is considered a constant-magnitude dead load. The load during the Riks step, on the other hand, is referred to as the reference load, and it is always proportional. The size of the present load may be described as follows:

$$F_{total} = F_0 + \lambda(F_{ref} - P_0) \quad (4)$$

F_0 is dead load, F_{ref} is the reference load vector, λ is proportionality factor. In ABAQUS/Standard, the Newton technique is utilised to solve nonlinear equilibrium equations. Along the static equilibrium direction, the initial increment in arc length Δl_{in} and initial lpf is $\Delta\lambda_{in}$.

$$\Delta\lambda_{in} = \frac{\Delta l_{in}}{l_{period}} \quad (5)$$

The overall length factor l_{period} is a set by the user during Riks step in its initial iteration is $\Delta\lambda_{in}$. The value is automatically computed for subsequent phases and accretions and λ and will have no control over

the magnitude of load. The automated increments are controlled by $\Delta\lambda_{min}$ (minimum arc length increment) and $\Delta\lambda_{max}$ (maximum arc length increment).

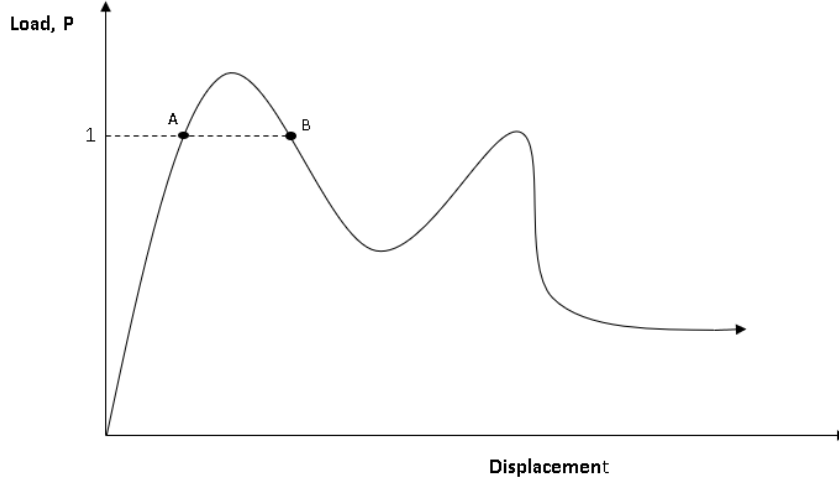


Figure 5: unstable response with proportional loading

Riks analysis has certain limitations, such as the fact that it cannot be followed by another evaluation phase. As a result, the very next steps must be re-evaluated. If there is an irreversible change, A Riks analysis includes factors such as plasticity. A restart utilising a entirely different Riks step is attempted when the strain on the structure reduces. The elastic unloading solution will be found by Abaqus/Standard. If plasticity is present, the analysis should be restarted at a point where the load magnitude is decreasing. The Riks method will usually not work for postbuckling problems involving loss of contact.

1.7.1 Arc Length Method

The Arc-Length method [10] is one of the most reliable ways of resolving solutions for non-linear systems of equations having one or more critical points. The point at which the body under load can no longer sustain an increase in external forces and instability occurs is known as a critical point in the context of a basic mechanical loading-unloading issue. Remember the non-linear (in general) equations we're attempting to solve:

$$P^{int}(w) - P^{ext} = 0 \rightarrow p^{int}(w) - \alpha r = 0 \quad (6)$$

The point (w_0, α_0) is such that the set of equations is satisfied, and hence belongs to the 'equilibrium' category. We're attempting to figure out what path to take. Unlike the Newton method, the Arc Length approach assumes that both displacements are changing at the same time Δw and the load vector coefficient $\Delta\alpha$. The major difference is that both Δw and $\Delta\alpha$ are unknowns in contrast to Newton's method where $\Delta\alpha$ was given and we had to iteratively solved for Δw . We can write

$$S(w', \alpha') = P^{int}(w_0 + \Delta w) - (\alpha_0 + \Delta\alpha)r = 0 \quad (7)$$

If the equation(1.7) is satisfied for $(w_0 + \Delta w, \alpha_0 + \Delta\alpha)$ then this location is on the 'equilibrium pathway,' and we may appropriately update the solution. Because quick compliance of equation (1.7) is not possible in most instances, we must give adjustments $(\delta w, \delta\alpha)$ such that new point $(w_0 + \Delta w + \delta w, \alpha_0 + \Delta\alpha + \delta\alpha)$ will satisfy equation(1.2) such that

$$S(w'', \alpha'') = P^{int}(w_0 + \Delta w + \delta w) - (\alpha_0 + \Delta\alpha + \delta\alpha)r = 0 \quad (8)$$

By using a Taylor series expansion and only retaining linear terms thus we can rewrite the above equation in the form of

$$P^{int}(w_0 + \Delta w) + \left[\frac{\partial P^{int}(w)}{\partial w} \right]_{w_0 + \Delta w} \cdot \delta w - (\alpha_0 + \Delta\alpha + \delta\alpha)r = 0 \quad (9)$$

From now onwards $\left[\frac{\partial P_{int}(w)}{\partial w} \right]$ is represented as "Jacobian matrix" of the system and which in turn is represented by the quantity $[J_T]$ and now the above equation can be written as

$$[J_T]_{w_0 + \Delta w} \cdot \delta w - \delta \alpha r = -[P^{int}(w_0 + \Delta w) - (\alpha_0 + \Delta \alpha)r] = -S(w', \alpha') \quad (10)$$

Here δw and $\delta \alpha$ are the unknowns which needed to be solved. If vector w has dimensions $M \times 1$ and we have a total of M equations to solve for $M+1$ unknowns. So equation (1.5) is not sufficient to find out $\delta u, \delta \alpha$. The Arc Length Equation is a supplementary equation that completes the system and has the following form:

$$(\Delta w + \delta w)^T \cdot (\Delta w + \delta w) + \psi^2 (\Delta \alpha + \delta \alpha)^2 (r^T \cdot r) = \Delta l^2 \quad (11)$$

ψ and Δl are user defined parameters, Δl is the arc length increment and it is comparable to load increment $\Delta \alpha$ used in Newton's method. The above equations (1.5) and (1.6) can be written as matrix form as follow as

$$\begin{bmatrix} [J_T] & -r \\ 2\Delta w^T & 2\psi^2 \Delta \alpha (r^T \cdot r) \end{bmatrix} \cdot \begin{bmatrix} \delta w \\ \delta \alpha \end{bmatrix} = - \begin{bmatrix} S \\ A \end{bmatrix} \quad (12)$$

where,

$$\begin{aligned} S &= P^{int}(W_0 + \Delta W) - (\alpha_0 + \Delta \alpha)r \\ A &= -(\Delta w^T \cdot \Delta w + \psi^2 \Delta \alpha^2 \cdot (r^T \cdot r) - \alpha l^2) \end{aligned}$$

Equation (1.7) is solved for $\delta w, \delta \alpha$ and updates the previous corrections $\Delta \alpha, \Delta w$ to be $\Delta w' = \Delta w + \delta w$ and $\Delta \alpha^{prime} = \Delta \alpha + \delta \alpha$. The method provides such incremental corrections $\delta w, \delta \alpha$ until convergence is achieved.

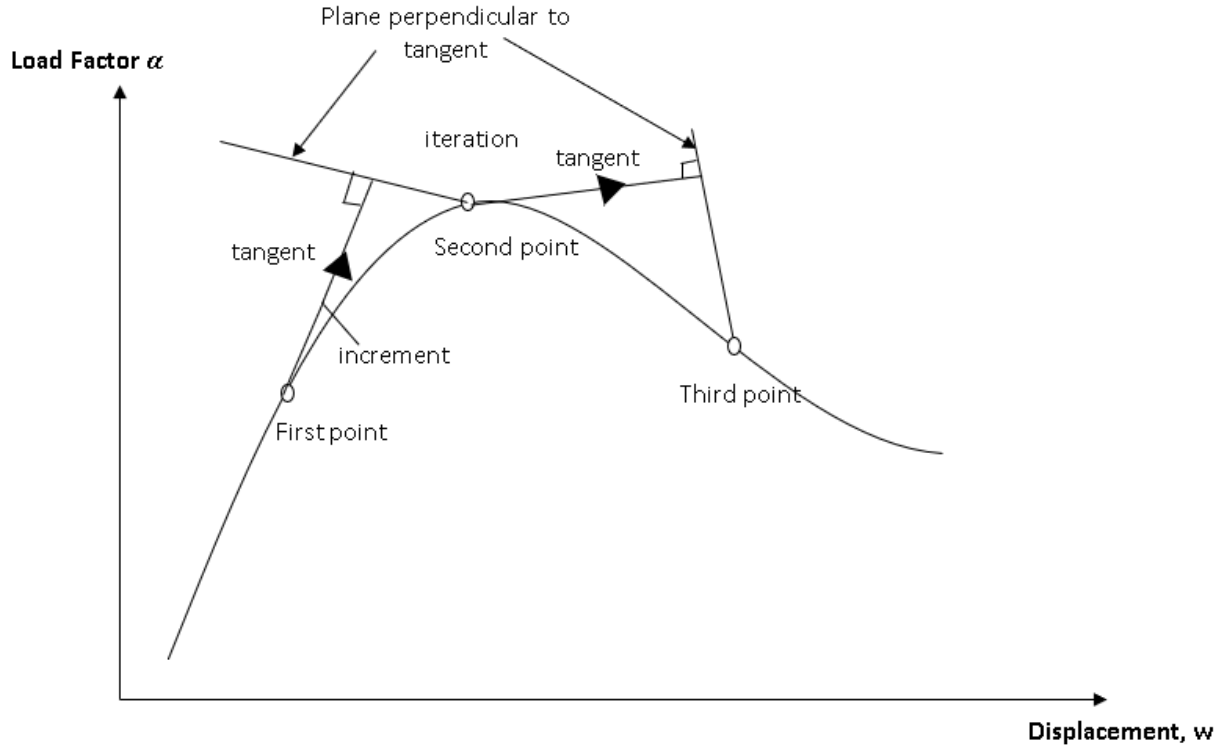


Figure 6: Arc length technique

1.8 Procedure for simulation in ABAQUS

Fig shows the flowchart to simulate the problem in ABAQUS simulation consists of mainly two steps. First step is preparation of model which includes creation of sketches, parts, assembly, mesh and the definition of boundary condition and load. The second step involves multiple sub steps initially buckling analysis using linear perturbation buckle is performed which gives us eigenvalues (buckling load) and eigenmode (buckling modes). Second sub step is post-buckling analysis it is done using static Riks procedure. Mostly post-buckling analysis is done using some imperfection in geometry. Imperfections are provided in the geometry as dimples or by scaling one or more buckling modes by some factor.

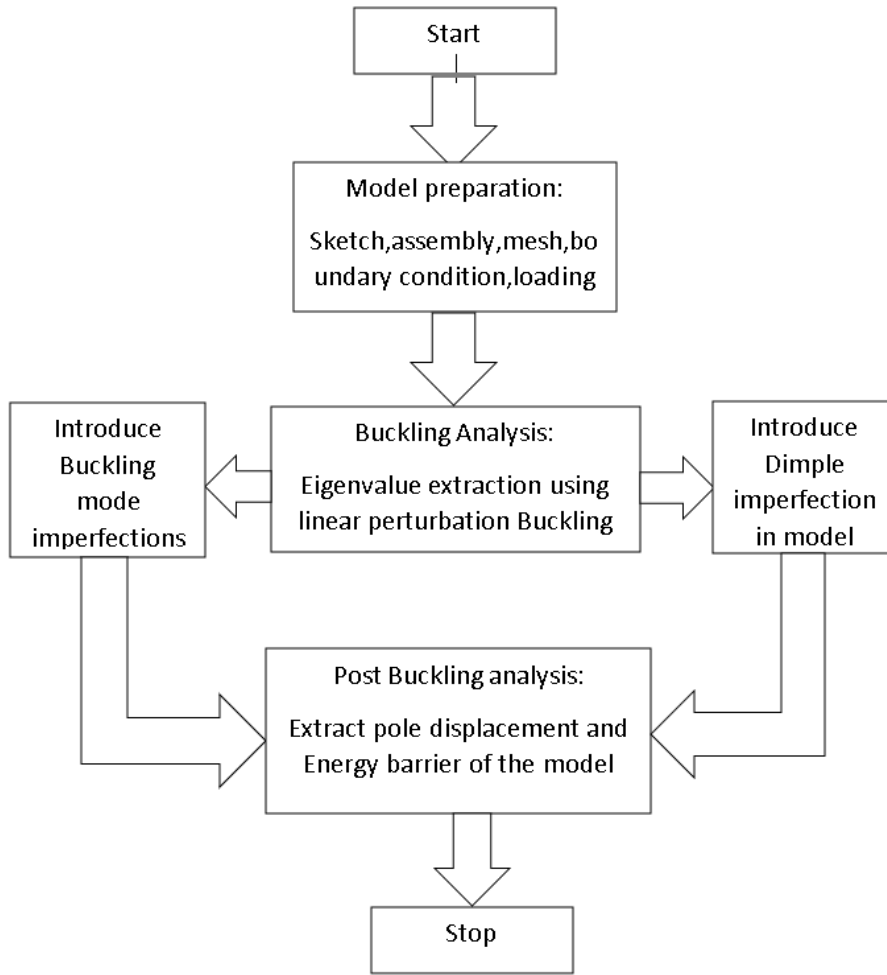


Figure 7: Flowchart for simulation in Abaqus

1.9 Co-ordinate systems

In our work we have used spherical coordinates for spherical shell to extract results. Vector and tensor quantities are computed with respect to 1,2 and 3 directions in 3D model. The 1,2, and 3 directions of converted findings correspond to the x,y, and z-directions of a rectangular coordinate system, according to the ABAQUS theory guide and the r, ω and θ of spherical coordinate system and in spherical coordinate system ω is the circumferential angle and θ is the meridional angle. Displacements are node based quantities and are calculated at nodes and pressure is element based quantity and are estimated at element centroid, element nodes and element face.

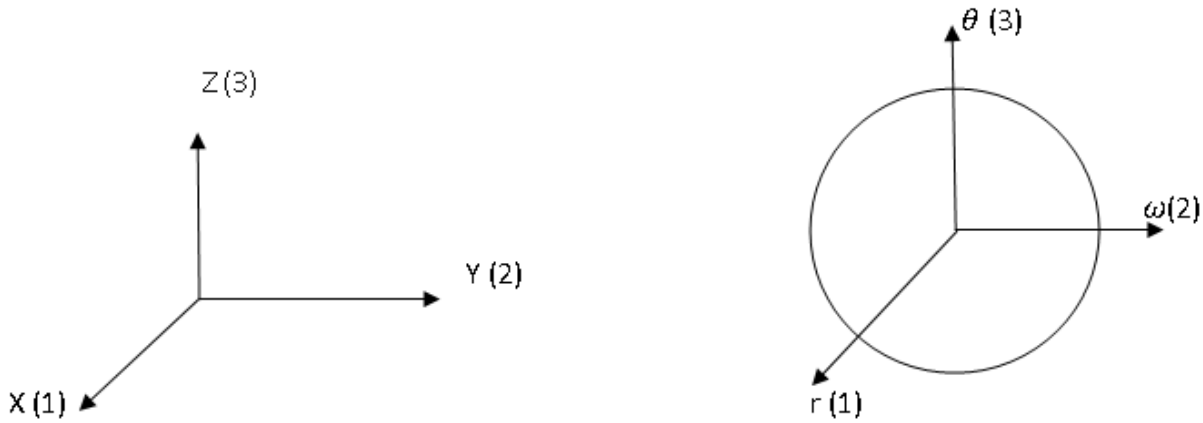


Figure 8: Cartesian and spherical coordinate system

2 Spherical Shell

2.1 Motivation

In our work we are motivated by the lack of knowledge regarding to relation of geometric imperfection to maximum buckling load of thin shells and also knock down factor is heavily used in designing imperfect spherical shells accounting for imperfections on the surface of spherical shell as a result the buckling load is reduced below the projected value.. This approach ensures that shell will not buckle the value below the buckling load but it does not give an idea about the robustness of a pre-loaded shell subjected to accidental loads. To assess the robustness our analysis is focussed on energy limit that exists below the buckling load. Furthermore, we will also able to see the buckling mode localization immediately after bifurcation

2.2 Problem formulation

Using the ABAQUS/STANDARD package, the condition of spherical shell struture under uniform external pressure is simulated . Displacement and load boundary conditions are defined with respect to cartesian coordinate system during pre-processing in ABAQUS. Then we use spherical coordinate system is used for post processing.

2.2.1 Boundary condition and Loading

Around the vertical axis, the spherical shell is assumed to be symmetric with θ representing the meridional angle which varies such that $\theta = 0^\circ$ at equator and $\theta = 90^\circ$ at the pole and the hemisphere shell is completely fixed at the equator and uniform external pressure is acting on the surface of the shell as we can see in the

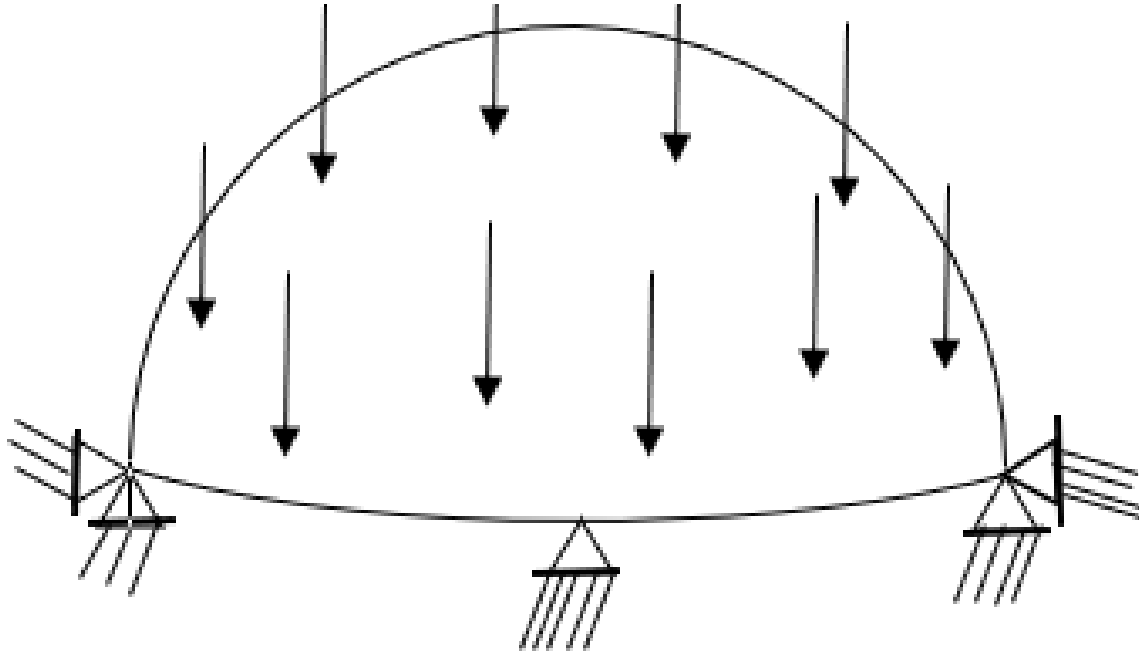


Figure 9: Loading and Boundary condition representation

property	values
Density	7850 kg/m ³
Poisson's ratio	0.3
Young's Modulus (E)	210 GPA

Table 1: Material Properties

Fig 9.

Shell structure is allowed to deform in any direction that is no displacement boundary conditions are given. Boundary conditions specified are:

Translational boundary conditions: $U_1 = U_2 = U_3 = 0$

Rotational boundary conditions: $Ur_1 = Ur_2 = Ur_3 = 0$

2.3 Material Properties

It is assumed that the material is linearly elastic, isotropic, and homogeneous and the material remains elastic and plastic behaviour never occurs. Material properties are mentioned in the below table. The value of density is chosen to be higher as it does not play any role in buckling and static analysis. While in the case of dynamic analysis with no rigid body motion higher density helps in faster analysis without affecting the results.

2.4 Modelling and Simulation Procedure

We have used ABAQUS/CAE 2017 for finite element analysis. The simulation is done in steps discussed below.

Step – 1:

We will be creating axisymmetric hemispherical shell in part module using axisymmetric deformable shell options and three shell models are created with different radius $R = 100, 200, 300$ mm and thickness of shell

is same for all the models that is $t = 1\text{mm}$. Material properties and sections are assigned to the model

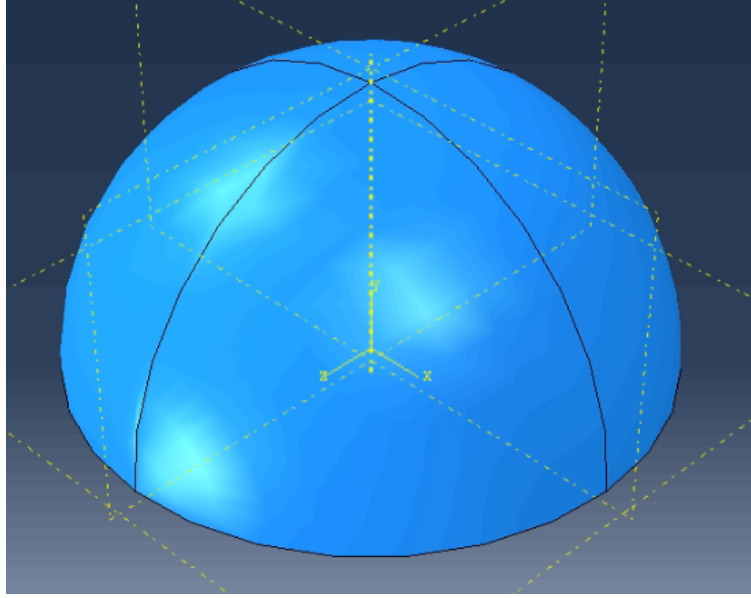


Figure 10: Shell Model

Step-2:

The model is meshed using reduced hybrid axisymmetric elements CAX4RH with reduced integration and hour glass control. We have generated 15360 elements to arrive at this we have performed mesh convergence.

Step – 3:

In this step in load module, we define boundary conditions which is in symmetry option we will be choosing encastre option which completely fixes the shell. We then use linear perturbation step, buckle, for eigenvalue analysis. Then the buckling load and buckling modes (eigen modes) are extracted.

Step-4:

We will be introducing buckling mode imperfections first by using first buckling mode or classical mode imperfections and scaled accordingly. The second type of imperfections are the dimple imperfections which are introduced at the pole. The post buckling analysis will be performed on the model with geometric imperfections.

Step 5:

Now post-buckling analysis is performed which is done using Static Riks method which handles instability or bifurcation problems very well and gives us good results.

2.5 Mesh

Meshing of the model has been done manually using quadrilateral elements i.e., CAX4RH with reduced integration and hourglass control, hybrid with constant pressure. Reduced-integration allows linear to have only one integration point at the element's centroid. When calculating the integral, reduced integration employs a smaller number of Gaussian co-ordinates. We would have significantly reduced time taken for analysis but accuracy will be reduced. Whenever we use reduced integration while post processing, we may experience false or fake deformation (zigzag lines) this is called hourglass effect. The reason for phenomenon of hour glass effect is because elements with lesser integration points are less stiff and as there is no stiffness in this mode, these elements have shown this kind of change in Configuration. So, we will be using hourglass control option to reduce this effect.

2.5.1 Types of Elements

Two types of elements can be used the quadrilateral elements has four control points and triangular element has three control points. Quadrilateral elements are preferred when the geometry is curved surface and quadrilateral elements gives relatively accurate results, and are more used in complex systems in general. So, we have used quadrilateral elements.

Quadrilateral Bilinear Element (CAX4RH): These are four noded elements Each node of quadrilateral element has three displacement and three rotational degree of freedom and each component of displacement and rotation is linear in each direction, i.e., each component is a bilinear function across the element. In ABAQUS, these shell elements with reduced integration have code CAX4RH.

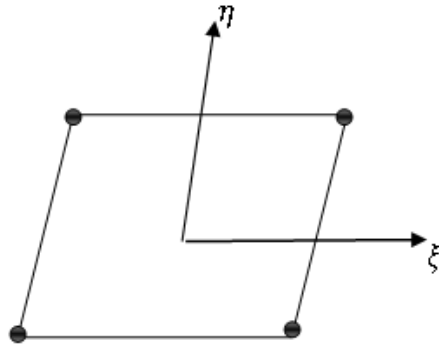


Figure 11: Quadrilateral Element

Triangular Linear Element (CAX3H): Triangular elements have three nodes. Each and every node has three displacement and three rotational degree of freedom and displacement and rotation components vary linearly across the element.



Figure 12: Triangular Element

2.5.2 Procedure for Meshing

In our problem as our model is axisymmetric and uniform hemispherical shell, we will be using structured mesh as it provides implicit connectivity and allows for easy identification of elements and nodes and we

having less complex geometry. Structured mesh provides fast and memory efficient solutions. Then the number of elements or mesh size is decided upon the accuracy which is needed. We must also check that the analysis' results are unaffected by the mesh size change. Mesh convergence can be accomplished by plotting the crucial output parameter (pressure) against the number of elements in the mesh and number of convergence runs are three which are performed and plot the curve which is used to illustrate convergence. If two runs for different number of elements are performed and if the results are very close then we say convergence is achieved.

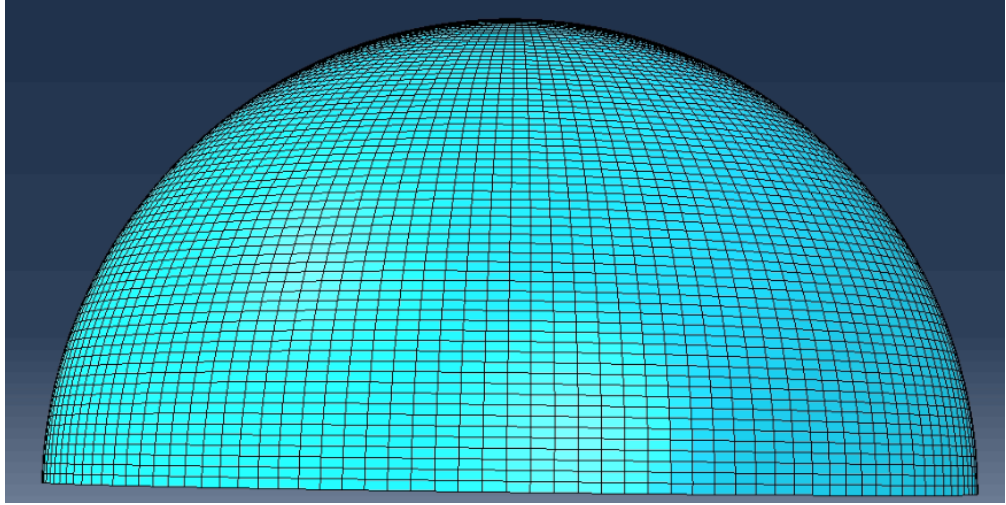


Figure 13: Mesh of shell struture with 3910 elements

We have performed geometrically nonlinear analysis for different mesh sizes and plotted against the buckling load(P) against total number of elements in Fig.14. Based on the plot we have chosen mesh size with 3910 elements which gives buckling load 23.9073 Mpa. So the buckling load value does not change beyond this and achieves convergence so we will be choosing this mesh size to balance out between convergent results and computational resources as beyond this it takes very long time to obtain results without significant difference.

2.6 Buckling Analysis

Linear perturbation buckling step in ABAQUS is an eigen value analysis. It is done with BUCKLE keyword and subspace solver and subspace iteration solver is faster only when few eigen modes are needed. Buckling load can be calculated (P_{bi}) as follows.

$$P_{bi} = \lambda_i P \quad (13)$$

Here λ_i is eigen value extracted from buckling analysis, 'i' is the mode number and P is the load value given in the load module. We will be specifying $P = 1$ hence $P_{bi} = \lambda_i$.

In the Fig.15 we can see first buckle mode. It is obtained after linear Buckling analysis and only shows only eigen mode not the real amplitudes of deformations, the other higher buckling modes with different wavenumber and buckling load.

Buckling load for first five modes have been listed in the below table. The first buckling mode gives us the lowest buckling load which will be used to specify the load in the further nonlinear analysis. Mode number(i) and Buckling load(P_{bi}) for first five mode numbers have been listed in the below table. The lowest buckling load has been observed for the first mode number and the load gradually increases for subsequent modes.

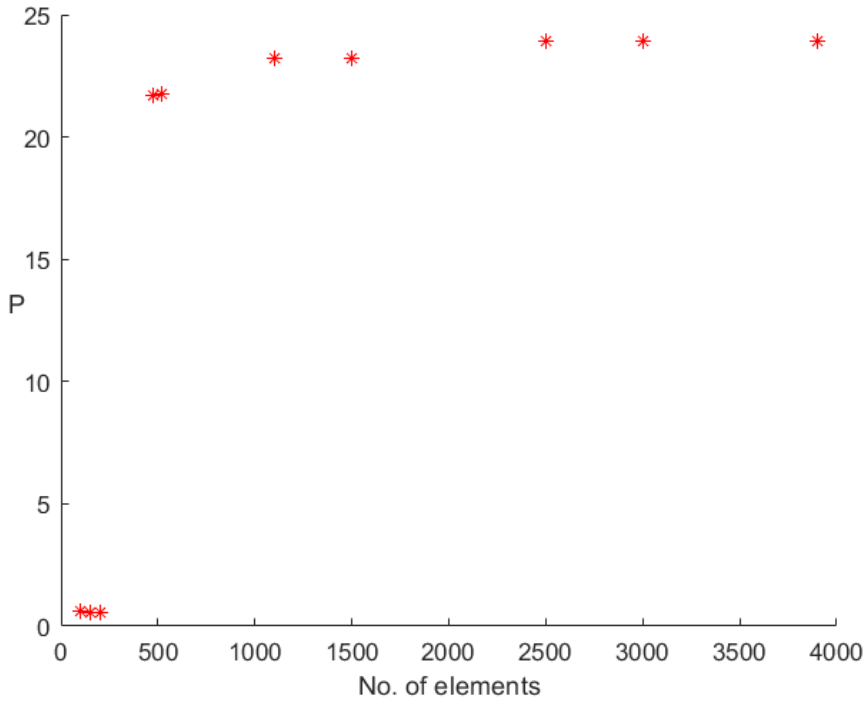


Figure 14: Plot of buckling load versus number of elements

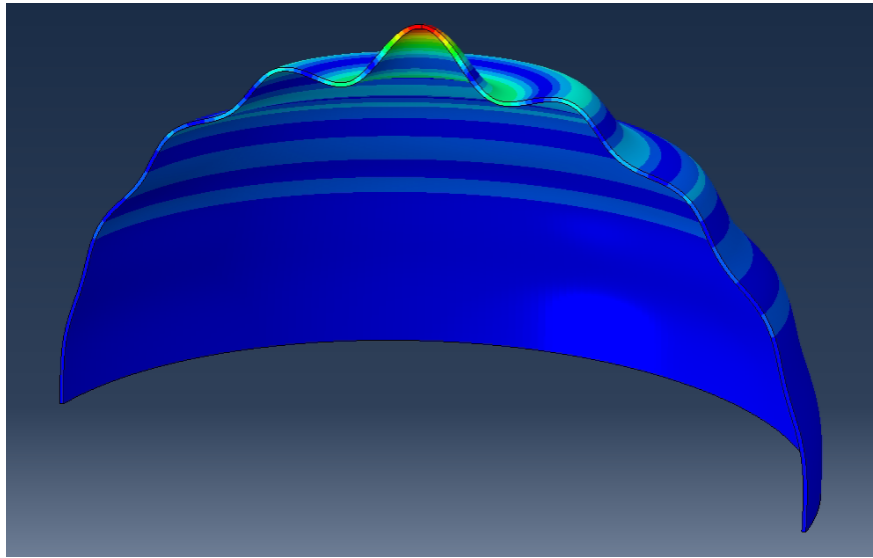


Figure 15: First Buckle mode for shell of $R/t = 100$

2.7 Buckling Analysis of Perfect Shell

In this section we will be focusing on geometrically nonlinear analysis of perfect shell. For geometrically nonlinear analysis of shell with radius $R = 100$ mm and thickness $t = 1$ mm i.e $R/t = 100$ and the shell material is assumed to be uniform, isotropic and linearly elastic and the material properties are Young's modulus $E = 210$ Gpa and Poisson's ratio $\nu = 0.3$. We will be using STATIC RIKS solver step and have considered geometric non linearity by selecting option "Nlgeom = on". Applied load magnitude(P) is equal to

Mode(i)	Buckling Load(P_{bi})
1	25.248
2	25.692
3	26.454
4	27.398
5	28.912

Table 2: Buckling load and mode number for shell with $R/t = 100$

the 25.248 Mpa that is load in first buckling mode and pressure applied is uniform throughout the spherical shell surface and the boundary conditions are specified same as which are specified in the linear buckling analysis.

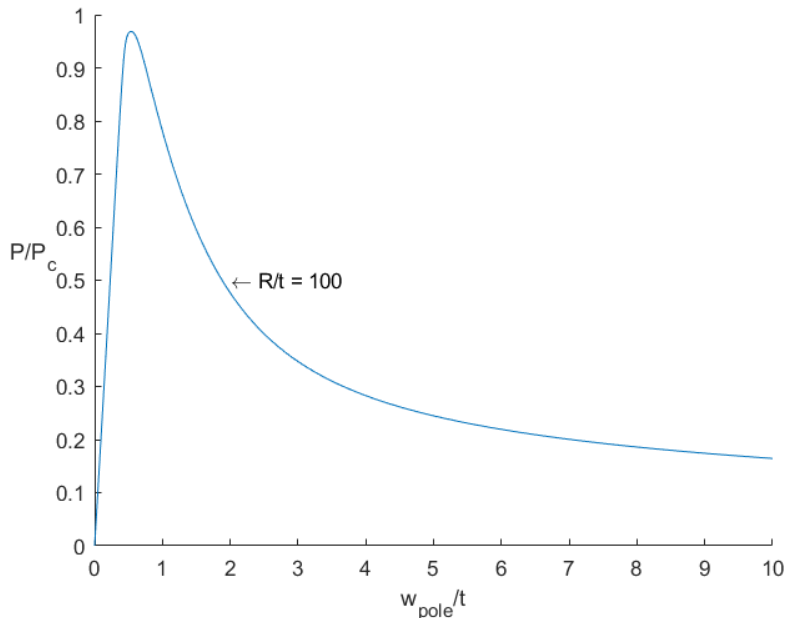


Figure 16: Post Buckling behaviour of perfect shell for small range of deflections for $R/t = 100$

In the Fig 16 of pressure ratio versus pole deflection normalized by shell radius obtained from the simulation results of geometrically nonlinear analysis gives us the nonlinear elastic buckling pressure of 24.613 Mpa and knockdown factor of 0.9683 and in comparison to critical pressure from classical buckling condition the buckling pressure is reduced by 3.17% (as per Eq:- $P_c = 25.419$ Mpa) and from the plot we can observe that the pressure increases sharply upto bifurcation point but after that the shell loading bearing capacity decreases with increase in pole displacement.

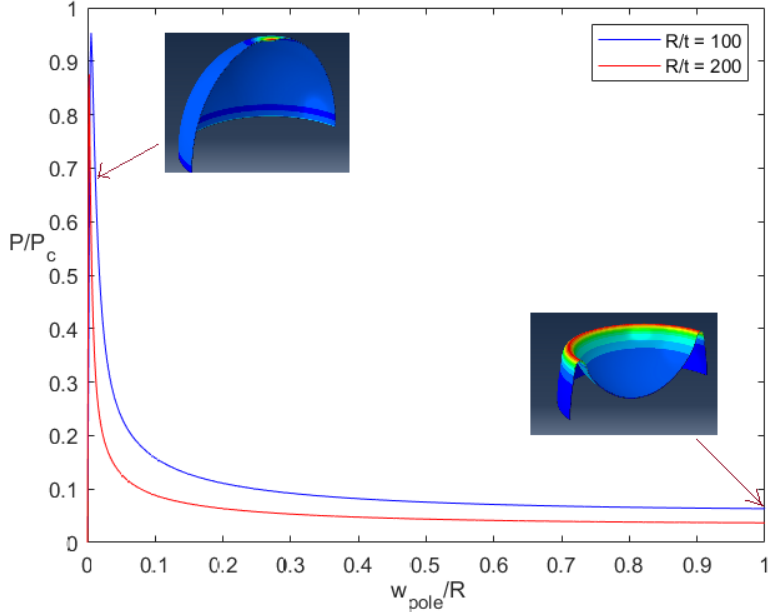


Figure 17: Pressure ratio versus pole deflection normalized by shell radius for large deformations insert figures show abaqus simulation for deformed surface

In Fig. 17 which is pressure ratio vs pole displacement normalized by shell radius we can observe the post buckling behaviour of shell where pressure monotonically decreases and in the insert figures we can observe the post buckling behaviour of shell where it's not resembling the classical axisymmetric mode but the deflections are concentrated at the pole which looks like an inverted cap similar results are also given in [11]. The deflections at the pole start immediately after the bifurcation and the magnitude of deflections increases such that opposing poles make contact. Following bifurcation during the post buckling behaviour the pressure always reduces to a point where the shell flattens out

Fig. 18 The axisymmetric normal deformations happening before buckling and after the buckling of an ideal shell fully fastened at the base are shown, in this Fig 18 we have paired the plot of pole deformation with the plot of full range of pressures. In each curve the upper part where($W/t > -0.55$) is called the "nodal" state (unbuckled state) in nomenclature of nonlinear dynamics which signifies stable response characteristics. The lower part of each curve ($W/t < -0.55$) represents saddle point (unstable buckled state). Buckling of shell occurs at the point $P = 0.9683P_c$ with $w_{pole} \approx -0.55$ establishing a link between the steady and unstable behaviors

3 Post-Buckling analysis of Imperfect Shells

3.1 Effect of Buckling mode imperfections

Defects are generally added to the geometry by perturbations Unless and until we are certain of the exact shape of the defect. We can introduce imperfection consisting of single buckling mode or multiple buckling mode superimposed. The The Riks approach may thus be used to evaluate structures that display linear behaviour prior to (bifurcation) buckling and evaluate after they have buckled. Linear perturbation is the eigen value buckling analysis and it is a linear analysis, imperfections are added for the nonlinear analysis is to be performed. The procedure for specifying eigen mode imperfections is as follows:

Step 1:

As nodal data, add the eigenmodes to the results file in the default global system. Step 2:

Eigen modes are then superimposed as imperfections to the perfect shell, and the 1st mode shape is associated large scale factor. In most cases, the scaling factor is calculated as a multiple of the geometry parameters.

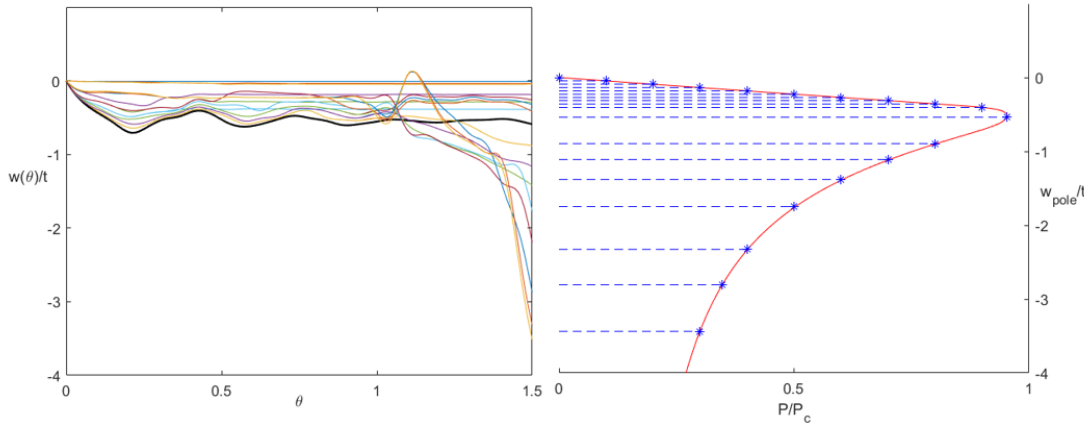


Figure 18: Pressure versus pole deflection normalized by shell radius, insert figures are from abaqus simulation showing deformations

Choice of selection scaling factors must be made in such a way that (assuming the structure isn't susceptible to defects) the factor for the lowest buckling mode should be the largest. Typically, just a few percent of a relative structural dimension, such as beam cross-section or shell thickness is altered.

Step 3:

To perform post-buckling analysis either ABAQUS/Standard or ABAQUS/Explicit can be used in our problem So, using Riks technique, post buckling analysis on "stiff" shells with linear behaviour before to buckling may be performed.

For defining an imperfection based on eigenmode data we need to edit .inp file of the job. This can be done in both ways first by opening .inp file in notepad or by using Edit Keyword option in Abaqus CAE interface. First in order to use eigenvalue file, the keywords of linear buckling analysis file should be modified first and we add these below keywords before *End Step keyword

*node file

*U

and after adding these we need to edit keywords in nonlinear analysis file here we will specify the buckling mode and scaling factor. The following keywords are added just after the *End Assembly.

*IMPERFECTION,FILE='job name',Step=1

1,0,1

Above we have specified first buckling mode and the scaling factor 0.1 represents 10% of the shell thickness here 0.1mm and in place of job name we should specify our name give to job of linear buckling analysis. Fig 19 represent the plot of normalized pressure vs normalized pole deflection for spherical shell with eigenmode imperfections with four different imperfection amplitudes. At the applied pressure p_{max} , the shell would become unstable and undergo buckling. We can also clearly observe that for imperfection amplitudes upto 0.1 the p_{max} occurs at $w_{pole}/t < 1$ and for $\delta = 0.25$ the p_{max} occurs at $w_{pole} > 1$. As the imperfection amplitude is increasing there is pressure drop taking place. The pressure drop is not that significant for small imperfection amplitudes, but as the imperfection amplitude is 0.1 the peak pressure is 16.606 Mpa and the drop from classical estimation is 34.67% which is a significant pressure drop as the imperfection amplitude increases to 0.25 again there is a drop of 62.46% from classical pressure estimation. In the Figure 20 we can see that immediately after the snap buckling the deformations are uniform throughout the shell surface and during post-buckling stage the deformations begin to localize at the pole of shell. The buckling deformation amplitude at the pole is greater than at other places following the bifurcation for a spherical shell experiencing axisymmetric deformation, this increase in amplitude of deformations at pole has very less similarity to eigen buckling mode, for this reason during post-bifurcation buckling mode deformations have small range of validity.

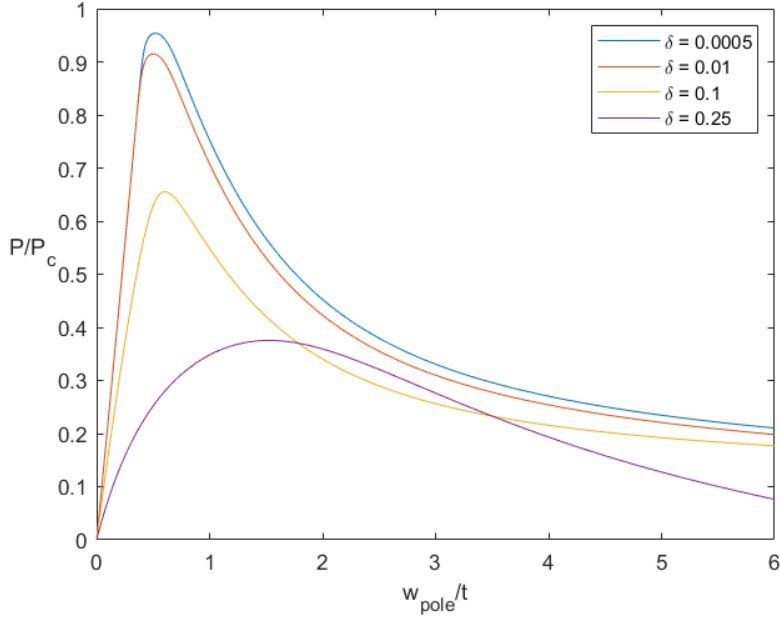


Figure 19: Plot for pressure ratio versus pole deflection normalized by shell thickness for different imperfection amplitudes for preloaded shell with eigenmode imperfections

3.2 Effect of Dimple Imperfections

The buckling mode deformations increasing at the pole has refocused our focus on the shell's axisymmetric behaviour, but this time look for dimple-shaped defects at the poles, as shown by

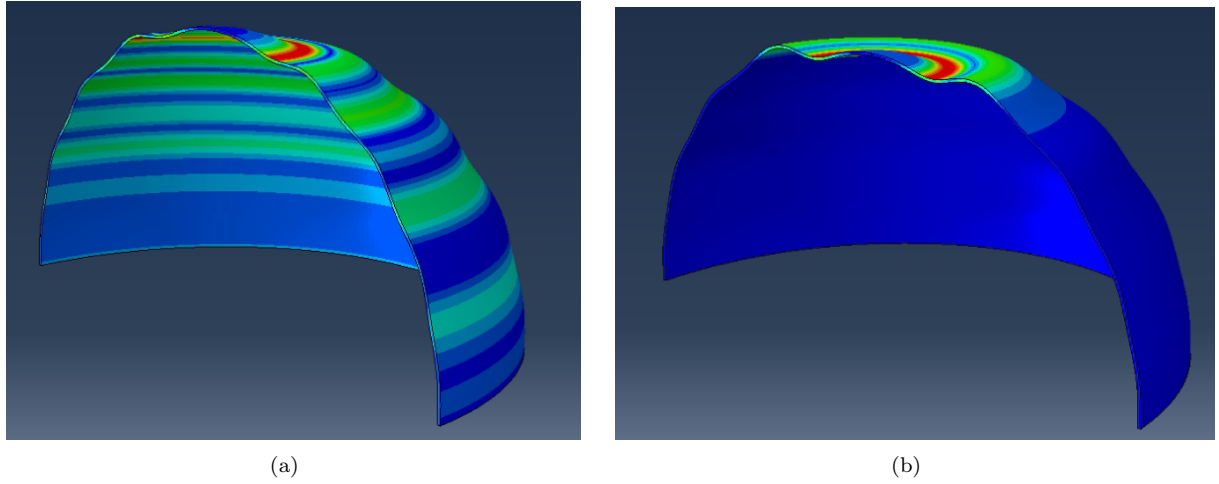
$$w_I(\theta) = -\delta e^{-(\beta/\beta_{ref})^2} \quad \text{with} \quad \beta = \theta - \pi/2 \quad (\text{at the upper pole}) \quad (14)$$

Here β_{ref} denotes the imperfection width [12]. Imperfection becomes increasingly tiny for $\beta \gg \beta_{ref}$ and is zero near the equator in the majority of situations. The symmetrical deflections around the equator will be the focus of our research, this increased deformations nature of buckling distinguishes behaviour above and below the equator. In general, the symmetric condition with identical defects at each pole and the asymmetric condition have the same imperfection susceptibility.

$$\beta_{ref} = \frac{B}{(\sqrt{1 - \nu^2} R/t)^{1/2}} \quad (15)$$

Fig 21 we have plotted normalized pressure versus normalized pole deflection for various imperfection amplitudes for smaller imperfection amplitudes the pressure reduction is small but for the larger imperfection amplitudes the pressure reduction is significant, and after snap buckling the pressure decreases monotonically.

In the Fig 23 we have plotted normalized maximum pressure versus normalized imperfection amplitude in the Fig 23(a) we have plotted for various imperfection widths and in the 23(b) we have plotted for varied radius to thickness ratio. So from the 23(a) we can observe that the largest pressure reduction takes place for wider imperfection. In all the cases in the Fig 23 P_{max} is associated with well denoted maximum pressures, like those seen in Figure 3.1, that occur at smaller pole deflections. with $B = 2$ and $\delta/t > 1.6$ being the lone exception. Where we could not see clear peak at smaller deflections. If a maximum pressure occurs in these circumstances, If there is no maximum pressure, P_{max} is either the peak pressure or the pressure at $w_{pole}/t = 5$.



(a)

(b)

Figure 20: Cross-section image of deformations of shell under eigenmode imperfections and $\delta = 0.25$ and (a) pressure ratio is 0.364, and (b) pressure ratio is 0.164

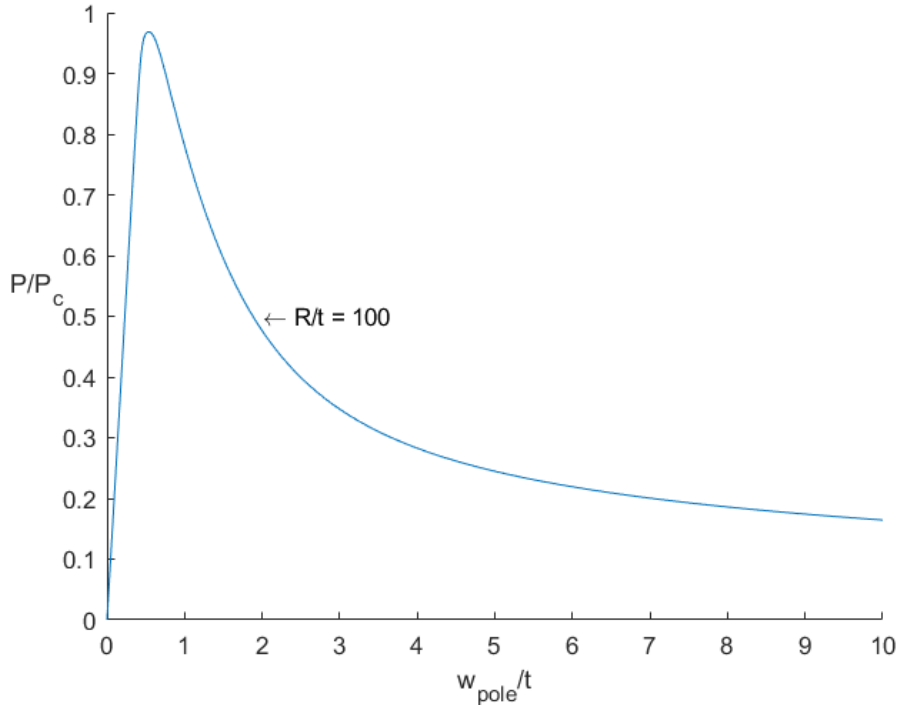


Figure 21: Plot for pressure ratio versus pole deflection normalized by shell thickness for different imperfection amplitudes for preloaded shell with dimple imperfections

From the Fig 23 for shells with dimple defects specified by width $B = 1.5$, demonstrates again that it does not depend on radius to thickness ratio as long as the imperfection widths are scaled according to the (3.2).the lower limit or plateau which is at $P_{max}/P_c \approx 0.35$, is a notable property of this imperfection susceptibility, for buckling when imperfections are of large amplitudes,independent of Radius to thickness ratio. The plateau behaviour provides crucial conclusions for determining the reduction factor during buckling spherical shell structures, which will be explored in more detail in the next sections, and this plateau behaviour was also

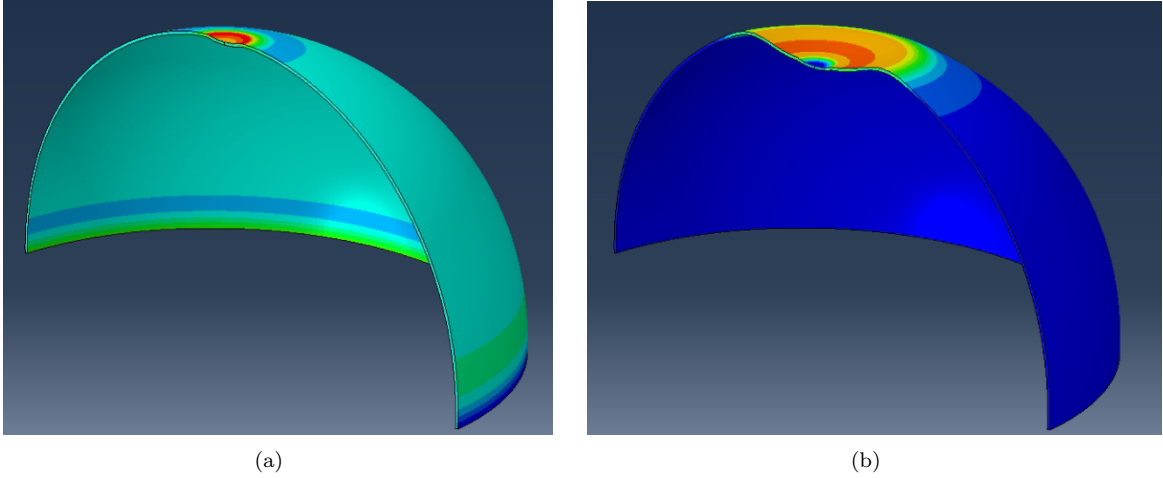


Figure 22: Cross-section image of deformations of shells under dimple imperfections and (a) immediately after buckling, and (b) further in post buckling range

discussed in [13].

3.3 Energy Barrier For Buckling Of Spherical Shells

When designing imperfection-sensitive spherical shell structures under external pressure, By decreasing the projected critical load below the expected load for a defect less structure, the knock-down factor is utilized to account for structural defects. While this method ensures that the shell does not buckle when the load is less than the knocked-down amount, but it does not provide knowledge on how resistant a loaded shell is to impact or accidental loading. We'll concentrate mostly on the energy limit that occurs at loads lower than the critical load. to determine the robustness of imperfection-susceptible shells under buckling phenomena. The energy limit to buckling for a shell with behaviour taking place after buckling at a given respective loading condition is the difference between the energy of the structure at buckled state and the energy of the shell in its unbuckled state. Only disruptions with energies greater than or equal to energy limit can cause buckling in the buckled state. The state with the least energy must be found in systems having several buckled states under a given load to use this concept. The energy barrier allows us to rationalise the energies of disturbances necessary to collapse the shell in a quantitative manner. At pressures below P_{max} , the quasi-static saddle buckling mode takes the shape of a dimple with axial symmetry at its centre. From simulations we can see that except at applied pressures just below P_{max} Near the centre of the emerging dimple buckle, the buckling behaviour is predominantly axially symmetric, and non-axisymmetric characteristics arise only well beyond the later part of the post-buckling range, which will not be studied in this study.

3.3.1 Energy barrier for buckling Of Perfect Spherical Shell

Fig 24 represents energy limit for buckling which is axially symmetric of a perfect elastic spherical shell completely fixed at equator subjected uniform external pressure. The following equation shows the volume change of a complete perfect spherical shell during bifurcation, commonly known as the classical buckling condition.

$$\Delta V_c = \frac{4\pi(1-\nu)R^2t}{\sqrt{3(1-\nu^2)}} \quad (16)$$

In Fig 24 the normalized energy barrier $E_b/[(P_c\Delta V_c/2)Ct/R]$ with $C = \sqrt{3}/[(1-\nu)\sqrt{1-\nu^2}]$, has been displayed as a function of the shell's normalised pressure ratio P/P_c , it has been calculated assuming axisymmetric behaviour about north-south pole axis of hemisphere. For thin spherical shells ($R/t \geq 100$) the post buckling deformations are confined to region of pole and has almost no interaction with the buckle on the clamped boundary. For thin spherical shells. For thin shells energy barrier does not depend on radius to

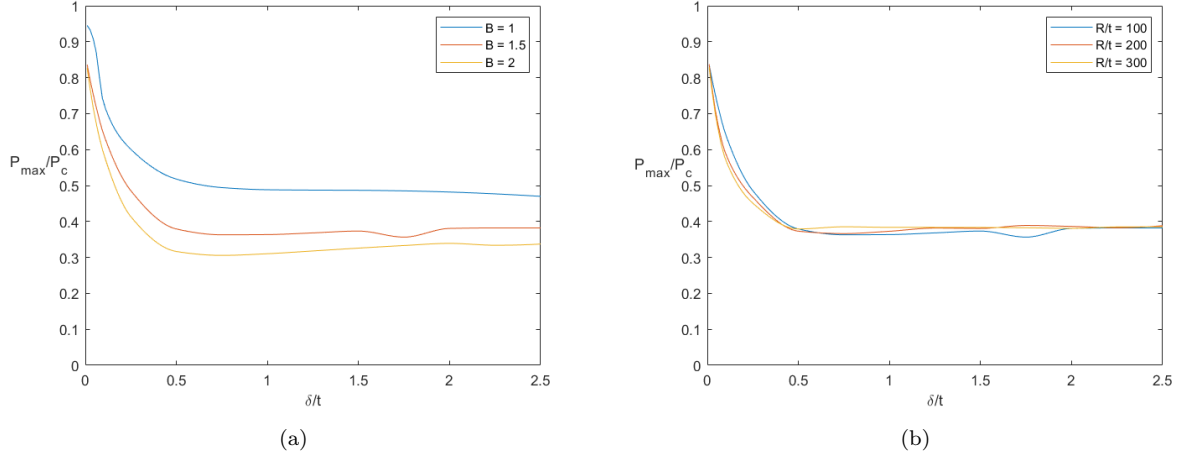


Figure 23: Plots for pressure ratio versus imperfection amplitude normalized by shell thickness (a) for three imperfection widths and $R/t = 100$, and (b) for three radius to thickness ratio and $B = 1.5$

thickness ratio and ν for $P/P_c \leq 0.85$. $(P_c \Delta V_c / 2) C t / R$ is a parameter that is used to normalise the energy limit it is the elastic energy in spherical shell at the classic bifurcation pressure $P_c \Delta V_c / 2$ where the term $C t / R$ is proportionate to the shell's thickness to radius ratio. From Fig 24 we can infer that energy limit is only a minimal percentage of total elastic energy except at lower applied pressures and also there is very minimal difference between energy limit for shells in the range of $P/P_c \leq 0.85$.

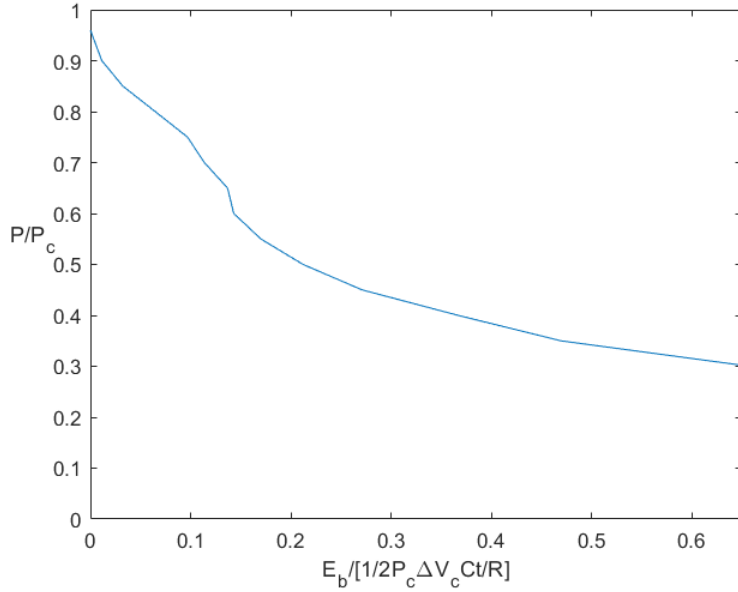


Figure 24: Plot of pressure ratio versus energy barrier normalized by elastic energy

3.3.2 Energy barrier for buckling Of Imperfection-Sensitive Spherical Shell Structure

The elastic spherical shells both the perfect and imperfect are exposed to an equal pressure all over the surface, The energy barrier against buckling is a useful criterion for evaluating the shell's buckling resistance to localized blast-like impacts. At the pre-loaded pressure, the quantity of energy associated with impact loads given to the shell must be greater than the energy limit. In the energy landscape, for impacts with

widths equivalent to the dimple buckle width connected with the saddle, the energy required to buckle the shell as a result of a collision may be only slightly more than the energy limit. Because the energy limit is very low, shells that have been pre-loaded to pressures nearer the pressure at buckling happens and with this amount of imperfection are hazardous. In the above section we have done analysis for perfect shell,

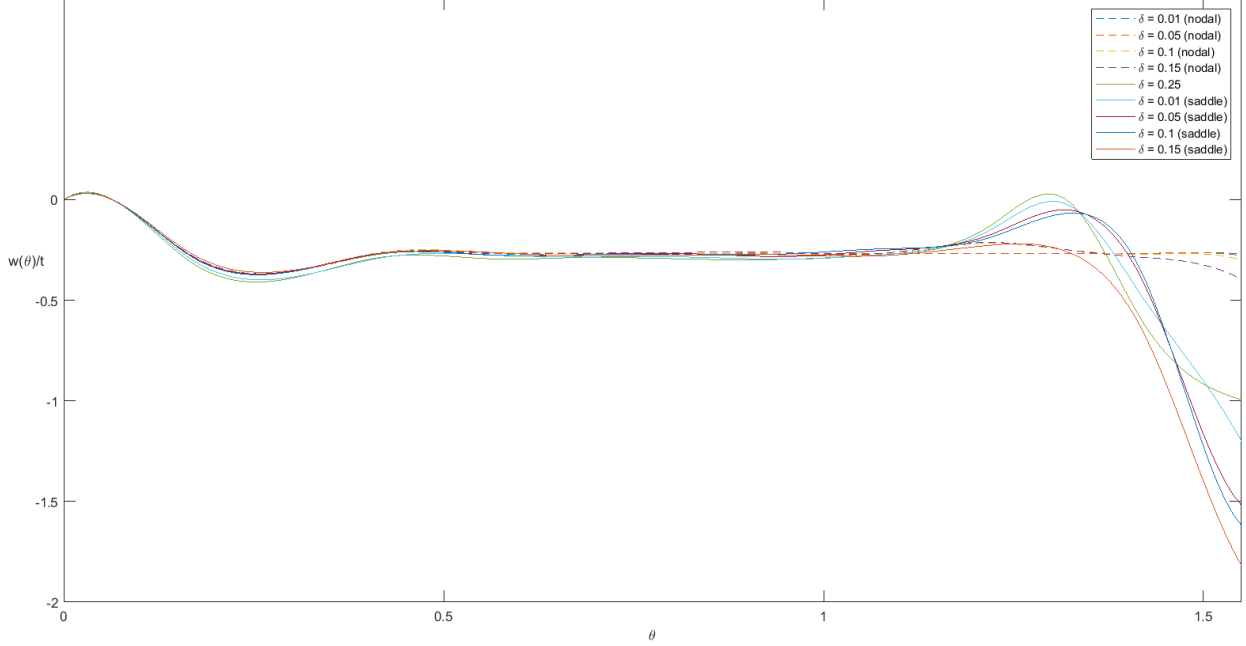


Figure 25: Plot of normalized radial deflection versus meridional angle for applied pressure ratio of $P/P_c = 0.5$ for different imperfection amplitudes

complete understanding of buckling energy barrier requires consideration of spherical shells with geometric imperfections under external pressure. Knockdown or maximum pressure P_{max} that can be supported by shell under uniform pressure is illustrated by imperfection widths given by Eq. 15 are $P_{max}/P_c \approx 0.83, 0.64, 0.38, 0.36$ for $w_{pole}/t = 0.01, 0.1, 0.5, 0.1$ respectively. These knockdown factors are applicable to hemispherical shells completely fixed at equator and does not depend on radius to thickness ratio for thin shells. To show the importance of early defects in the connection between the energy limit and maximum buckling limits under impact loads, we study a fully fixed hemispherical shell with defects which are present before. The shell is loaded to uniform pressure of $P = 0.5P_c$ and this is the maximum load shell can support for imperfections $\delta/t = 0.25$, so the range of imperfections considered here are $0 \geq \delta \leq 0.25$. Fig 25 presents us the results of deflection modes related to saddle and node states for the range of defect amplitudes we have considered above. From the Fig. 25 we can infer that nodal states are associated with $w_{pole}/t > -1.01$, meanwhile the saddle states are present at $w_{pole}/t < -1.01$ and the buckling deflection amplitude is becoming maximum in the region of pole. When imperfection amplitudes approaches nearer to the $\delta/t = 0.25$ When the nodal and saddle states merge, the energy limit disappears. This can be seen in Fig. 26 where it is consistent with the fact at this amount of imperfection shell is unstable for pre-load of $P = 0.55P_c$, and from the plot we can also infer that energy barrier E_b depends strongly on pressure ratio P/P_c and normalized imperfection amplitude δ/t .

subsectionConclusions and Future Work

3.4 Conclusions

We have simulated the buckling behaviour of spherical shell under uniform external pressure. In our work we have assumed that shell structure is empty without fluid. First we have performed linear buckling analysis and found out eigenvalues and eigenmodes for structure and after that we have performed o geometrically nonlinear analysis using STATIC RIKS solver on perfect shell and we can observe that pressure increases

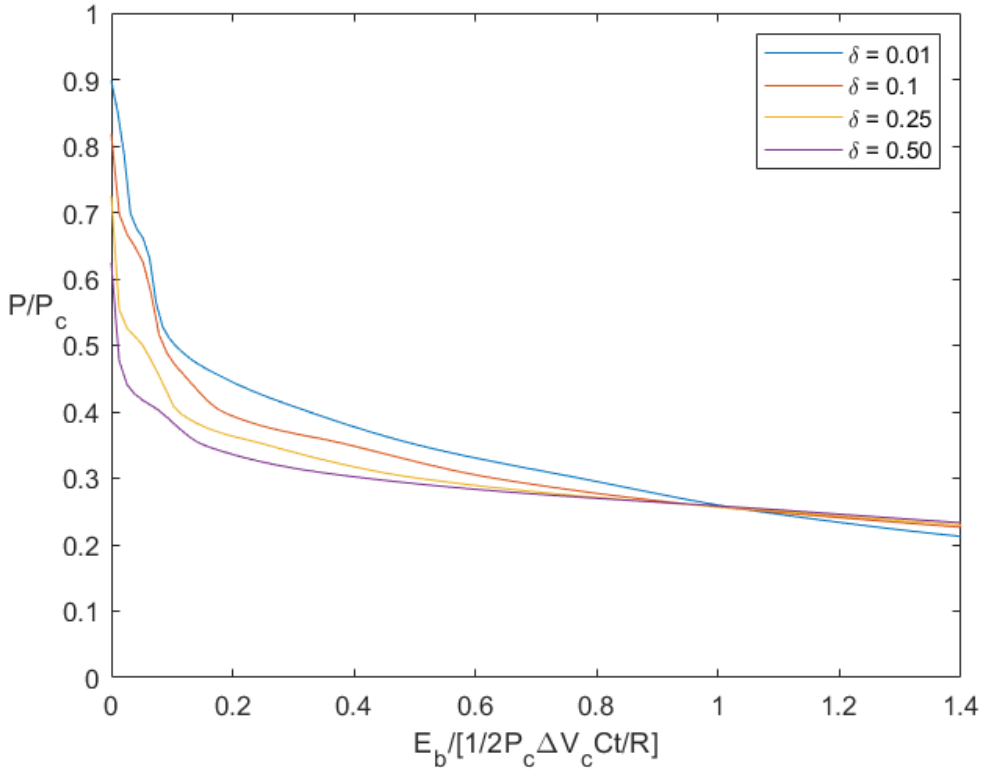


Figure 26: Energy barrier for spherical shell ($R/t = 100$) with dimple imperfections for different imperfection amplitudes

upto bifurcation point and shell buckles here and the load bearing capacity decreases with the increase in pole deflection and also we can observe that before buckling the deformations are uniform throughout the shell structure but as the buckling happens and in post buckling region the deformations are localized at the pole and as the deformations at $\theta = \pi/2$ increases in the post buckling range the pressure falls monotonically such that poles make contact, For perfect shell energy limit does not depend on radius to thickness ratio and ν and energy limit is negligible or small fraction of elastic energy for higher pressure ratios. We have also analysed a scenario where eigenmode is superimposed on the structure to simulate eigenmode imperfections behaviour here we have observed that for lower imperfection amplitudes the pressure drop is lower, as the imperfection amplitudes approaches value of 0.1 the pressure drop is significant. As during post buckling process of perfect shell we have observed that deformations are localized at the pole and are axisymmetric about the pole so we will be analyzing spherical shells with dimple imperfections the critical pressure the shell can sustain decreases as the imperfection amplitude increases and reaches a plateau at different pressure ratios for different imperfection widths and the load bearing capacity is does not dependent of radius to thickness ratio. The energy limit for shell with dimple imperfections is minimal at the higher pressure ratios and energy barrier does not depend on radius to thickness ratio and depends strongly on pressure ratios and imperfection amplitude.

3.5 Future work

In future the work can be extended for assumption that shell structure is filled with incompressible liquid, so that there will be an internal pressure due to liquid present inside the shell. These simulations with consideration of presence of liquid are very much closer to practical problems encountered. Where we may experience volume change due to internal pressure. Also we can consider imperfections all over the shell surface and not only at the pole, where these imperfections may reduce the buckling load.

References

- [1] T. Kármán, H. Tsien, The buckling of spherical shells by external pressure, *Journal of the Aeronautical Sciences* 7 (1939) 109–121. [2](#) [3](#)
- [2] W. T. Koiter, Over de stabiliteit van het elastisch evenwicht, 1945. [2](#)
- [3] J. Hutchinson, Imperfection sensitivity of externally pressurized spherical shells, *Journal of Applied Mechanics* 34 (1967) 49–55. [2](#)
- [4] J. Hutchinson, Buckling of spherical shells revisited, *Proceedings of the Royal Society A: Mathematical, Physical and Engineering Sciences* 472 (2016). [2](#)
- [5] R. Zoelly, Ueber ein knickungsproblem an der kugelschale, Ph.D. thesis, ETH Zurich, Zürich, diss. Techn.Wiss. ETH Zürich, Nr. 146, 0000. Ref.: Meissner, E. ; Korref.: Kollros, L.. (1915). [doi:10.3929/ethz-a-000091951](#). [3](#)
- [6] L. G. D. TH. VON KARMAN, H.-S. TSIEN, The influence of curvature on the buckling characteristics of structures, *Journal of the Aeronautical Sciences* 7 (1940). [3](#)
- [7] T. V. KARMAN, H.-S. TSIEN, The buckling of thin cylindrical shells under axial compression, *Journal of the Aeronautical Sciences* 8 (1941). [3](#)
- [8] D. Bushnell, Computerized buckling analysis of shells. mechanics of elastic stability, Vol. 9, Springer, Dordrecht, 1980, Ch. Descriptions of types of instability and classical buckling problems. [doi:https://doi.org/10.1007/978-94-009-5063-4_1](#). [3](#)
- [9] A. documentation MIT, [Unstable collapse and postbuckling analysis](#).
URL <https://abaqus-docs.mit.edu/2017/English/SIMACAEANLRefMap/simaanl-c-postbuckling.htm> [4](#)
- [10] E. Riks, An incremental approach to the solution of snapping and buckling problems, *International Journal of Solids and Structures* 15 (1979) 529–551. [5](#)
- [11] A. Evkin, M. Kolesnikov, D. A. Prikazchikov, [Buckling of a spherical shell under external pressure and inward concentrated load: Asymptotic solution](#), *Mathematics and Mechanics of Solids* 22 (6) (2017) 1425–1437. [arXiv:https://doi.org/10.1177/1081286516635872](#), [doi:10.1177/1081286516635872](#).
URL <https://doi.org/10.1177/1081286516635872> [15](#)
- [12] H. J. W. Sieber Jan, T. J. M. T., Nonlinear dynamics of spherical shells buckling under step pressure, *Proc. R. Soc. A.* 475(2018)0884 475 (2019). [doi:https://doi.org/10.1098/rspa.2018.0884](#). [17](#)
- [13] A. Lee, F. Lopez Jimenez, J. Marthelot, J. Hutchinson, P. Reis, The geometric role of precisely engineered imperfections on the critical buckling load of spherical elastic shells, *Journal of Applied Mechanics* 83 (08 2016). [doi:10.1115/1.4034431](#). [19](#)